EMBEDDING

1. Introduction

Advances in electronic technology have had great technological and economic impact on the electronic industry throughout the world. The rapid growth of the number of components per chip, the rapid decrease of device dimension, and the steady increase in integrated circuit (IC) chip size have imposed stringent requirements, not only on IC physical design and fabrication, but also in electronic packaging and embedding. Electronic embedding is one of the most common processes used to encapsulate and protect these electronic components. With advances in very large-scale integration (VLSI) technology and multichip modules packaging, embedding of this high density package in electronics has become a challenge (1–8). Various polymeric encapsulants are used for embedding these types of electronic components. These materials and their processes are discussed here in detail.

A discussion of a novel aluminum-filled composite for embedded passive applications is included.

2. Reasons for Electronic Embedding

The purpose of embedding is to protect the electronic components from adverse environments, from ~ -65 to 150 °C for military spec 883, thermal shock, temperature cycle during actual life applications, etc; improve handling in later assembly processes; protect line handling and impurities; and increase the long-term reliability of the electronics with a reasonable cost. High performance and low cost materials are the principal driving forces in the 1990s.

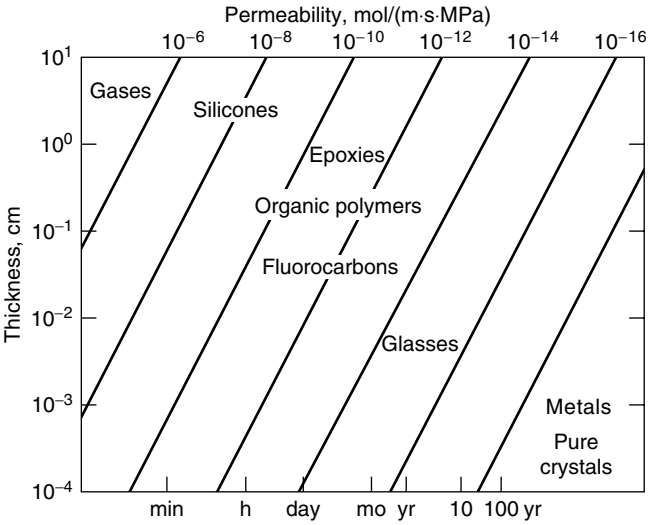

Fig. 1. Moisture permeability of various materials.

Electrooxidation (corrosion) and metal migration are attributed to the presence of moisture. When enough moisture diffuses through the encapsulant to form a continuous water path, with the presence of mobile ion(s) and under an electrical bias, electrocorrosion begins. Figure 1 shows the permeability of various materials. Pure crystals and metals are the best moisture barriers. Glass (silicon dioxide) is an excellent moisture barrier, but it is slightly inferior to pure crystals and metals. Organic polymers, such as fluorocarbons, epoxies, and silicones are a few orders of magnitude more permeable to moisture than glass. Silicone materials have the highest moisture permeability, yet they are one of the best device encapsulants. Obviously, gases are the most permeable to moisture of all materials, as shown in Figure 1. For each particular material the moisture diffusion rate is proportional to the water-vapor partial pressure and inversely proportional to the material thickness. This is accurate when moisture diffusion rates are in steady-state permeation. However, moisture transient penetration rates, perhaps more important because they determine the time it takes for moisture to break through, are inversely proportional to the square of material thickness.

Mobile ions, such as sodium or potassium, tend to migrate to the *p-n* junction of the IC device where they acquire an electron, and deposit as the corresponding metal on the *p-n* junction; this consequently destroys the device. Furthermore, mobile ions also support leakage currents between biased device features, which degrade device performance and ultimately destroy the devices by electrochemical processes such as metal conductor dissolution. For example, chloride and fluoride ions, even in trace amounts (ppm), could cause the dissolution of aluminum metallization of complimentary metal oxide semiconductor (CMOS) devices. CMOS is likely to be the trend of VLSI technology and sodium chloride is a common contaminant. The protection of these devices from the effects of these mobile ions is an absolute requirement. The use of an ultrahigh

purity encapsulant to encapsulate the passivated IC is the answer to some mobile ion contaminant problems.

Opaque encapsulants can protect light-sensitive optoelectronic devices from uv–vis light radiation damage. However, impurities in an encapsulant, such as traces of uranium in the ceramic or plastic package can cause appreciable alpha particle radiation, as can cosmic radiation in the atmosphere. Alpha radiation can generate a temporary "soft error" in operating dynamic random access memory (DRAM) devices and has become a significant concern, especially in high density memory devices. Good encapsulants must have alpha radiation levels less than 0.001 alpha particles/cm^2/h, and be opaque to protect from uv–vis radiation. Since alpha particles are weakly penetrating, a few micrometers thickness of encapsulant usually prevents this radiation damage to DRAM devices.

Hostile environments, such as extreme cycling temperature (values from -65 to $+150\,^{\circ}C$ in military 883 specs), high relative humidity (85 to 100%), shock and vibration, and high temperature operating bias are part of real life operation, and the device must survive these operation-life cycles. In addition, encapsulants must also have suitable mechanical, electrical, and physical properties, such as minimal stress and matching thermal expansion coefficient, etc, which are compatible with the IC devices. The encapsulant must have a low dielectric constant to reduce the device propagation delay, and excellent thermal conductivity to dissipate power-hungry, high speed bipolar IC and high density packages which generate tremendous amounts of heat that require special thermal management considerations. Furthermore, since the encapsulation is the final process step and some of the devices are expensive, particularly in high density multichip modules (MCM), it must be easy to apply and repair in production and service. With the proper choice of encapsulant and process, the embedding enhances the reliability of the fragile IC device, and improves its mechanical and physical properties and its manufacturing yields. These are the ultimate goals of the embedding (9–28).

3. Materials for Electronic Embedding

There are many polymeric materials with suitable electrical, chemical, and physical properties that could be used as electronic components embedding. However, only a few are widely used today.

3.1. Silicones. Polydimethylsiloxanes, polydiphenylsiloxanes, and polymethylphenylsiloxanes are generally called silicones (see SILICON). With a repeating unit of alternating silicon–oxygen, the siloxane chemical backbone structure, silicone possesses excellent thermal stability and flexibility that are superior to most other materials. Polydimethylsiloxane provides a very low glass-transition temperature T_g material but is suitable for use at temperatures up to $200\,^{\circ}C$. The basis of commercial production of silicones is that chlorosilanes are readily hydrolyzed to give disilanols which are unstable and condense to form siloxane oligomers and polymers. Depending on the reaction conditions, a mixture of linear polymers and cyclic oligomers is produced. The cyclic components can be ring-opened by either acid or base to become linear polymers and it is these linear polymers that are of commercial importance. The linear polymers are

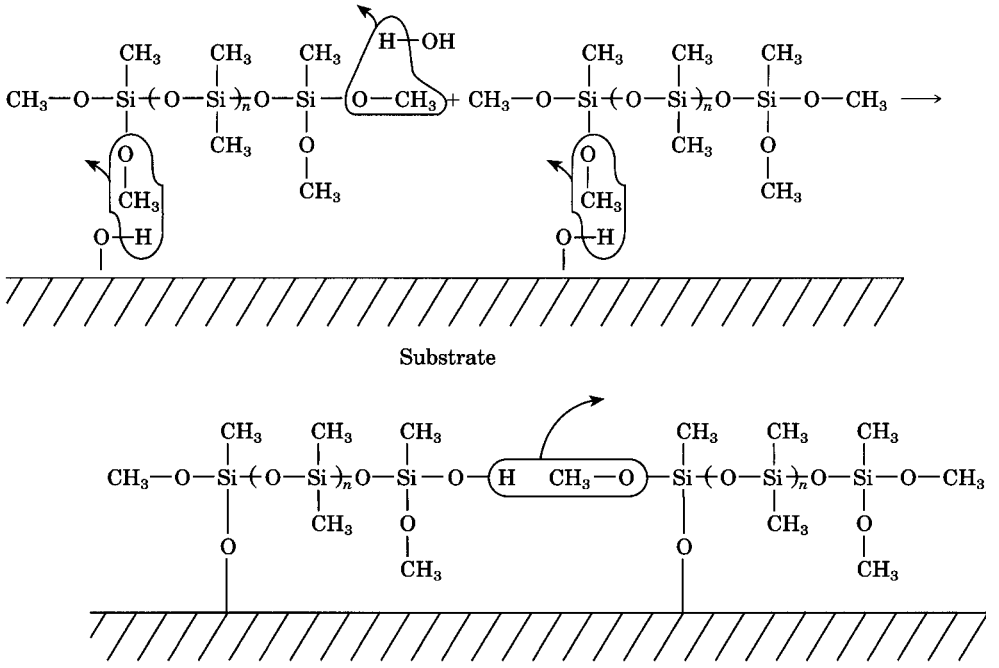

Fig. 2. Condensation-cure mechanism.

typically liquids of low viscosity and, as such, are not suited for use as encapsulants. These must be cross-linked (or vulcanized) in order to increase the molecular weight sufficiently to achieve useful properties. Three methods of cross-linking are used: condensation cures, addition cure systems, and peroxide free-radical cure systems. For electronic applications, only the high purity room temperature vulcanized (RTV) condensation cure silicone, which uses an alkoxide-cure system with noncorrosive alcohol by-products, and platinum-catalyzed addition heat-cure (hydrosilation) silicone systems are suitable for device encapsulation.

The moisture-initiated catalyst, such as organotitanate, tin dibutyl dilaurate, etc, assisted RTV process generates water or alcohol by-products which could cause outgassing and voids (Fig. 2). However, by careful control of the curing process, a very reliable encapsulant can be achieved (5–8,29,30). Since the silicone has a low surface tension, it tends to creep and run over the encapsulated IC circuits. To better control the rheological properties of the material, thixotropic agents, such as fumed silica, are usually added to the formulation. The thixotropic agent provides a higher yield stress material, increases the suitable G' (storage modulus), G'' (loss modulus), and η^* (dynamic viscosity) of the encapsulant. Filler–resin and filler–filler interactions are important in obtaining a well-balanced and well-controlled encapsulant. This rheological controlled material tends to flow evenly in each circuit edge, covers all the underchip area, and prevents wicking and runover of the circuits which is a critical parameter in coating production. In addition, pigments such as carbon black and titanium dioxide are

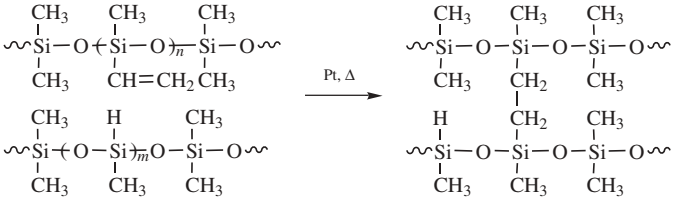

Fig. 3. Addition-cure mechanism, employing hydrosilyation involving a vinyl group and hydride; $m > n$.

usually added as opacifiers to protect light-sensitive devices. Organic solvents such as xylenes and Freons are incorporated into the formulation to reduce the encapsulant viscosity. That is probably one of the reasons why RTV silicone is capable of achieving superior performance in temperature–humidity bias (THB) accelerated electrical tests. Furthermore, the heat curable silicon–hydride and silicon–vinyl addition heat-cure system provides a fast and deep section-cure material system which is preferred in embedding of electronic components.

Heat-curable hydrosilation silicone (either elastomer or gel) has become an attractive device encapsulant (Fig. 3). Its curing time is much shorter than the RTV-type silicone. With its jelly-like (very low modulus) intrinsic softness, silicone gel is an attractive encapsulant in wire-bonded large-chip-size IC devices. The two-part heat-curable system which consists of the vinyl and hydride reactive functional groups, and the platinum catalyst hydrosilation addition-cure system provide fast-cure systems without any by-product. The key to formulating a low modulus silicone is the deliberate undercross-linking of the silicone system. A few parts per million (ppm) platinum catalyst such as chloroplatinic acid or organoplatinum is used in this system. This catalyst is usually incorporated in the vinyl portion of the resin. This solventless type of heat-curable silicone gel has an increasing use in electronic embedding. The ability of silicone gels to dampen shock and thermal stress is one of the reasons for their use in dedicated wire bonded or flip-chip bonded electronic components (12). Furthermore, the gels are also useful where failure or circuit analysis is needed. The gel allows a probe to be inserted to a test point and then removed; it "repairs" and reseals itself.

Silicon–Carbon Thermoset. The Sycar resins of Hercules are silicon–carbon thermosets cured through the hydrosilation of silicon hydride and silicon vinyl groups with a trace amount of platinum catalyst. The material is a fast-cure system ($<$15 min at 180 °C) and shows low moisture absorption that outperforms conventional thermosets such as polyimides and epoxies. Furthermore, the Sycar material provides excellent mechanical and physical properties used in printed wiring board (PWB) laminates and encapsulants such as flow coatable or glob-top coating of chip-on-board type applications.

3.2. Epoxies. The unique chemical and physical properties such as excellent chemical and corrosion resistances, electrical and physical properties, excellent adhesion, thermal insulation, low shrinkage, and reasonable material cost have made (see EPOXY RESINS) very attractive in electronic applications. The commercial preparation of epoxies is based on bisphenol A, which upon reaction

with epichlorohydrin produces diglycidyl ethers. The reactant ratio (bisphenol A:epichlorohydrin) determines the final viscosity of the epoxies. In addition to the bisphenol A resins, the novolak resins with multifunctional groups which lead to higher cross-link density and better thermal and chemical resistance have gained increasing acceptance in electronic applications. Typical epoxy curing agents are amines, anhydrides, dicyanodiamides, melamine–formaldehydes, urea–formaldehydes, phenol–formaldehydes, and catalytic curing agents. Anhydrides and amines are two of the most frequently used curing agents.

In most phenoxy resins, the phenolic group is converted into an ether to give improved base resistance. They are cured through the secondary hydroxyl group on the epoxy backbone. High temperature curing is required in this system and it provides excellent chemical resistance. Recently developed high purity epoxies contain greatly reduced amounts of chloride and other mobile ions, such as sodium and potassium, and have become widely used in device encapsulation and molding compounds. The incorporation of large loading (>70% by wt) well-controlled spherical silica particles of silicon dioxide with narrow size-distribution as filler in the epoxy systems has drastically reduced the thermal coefficient of expansion of these materials and makes them more compatible with the IC die-attached substrate materials. The incorporation of a small amount of an elastomeric material, such as silicone elastomeric, carboxyl-terminated butadiene (CTBN) type domain particles, to the rigid epoxy has drastically reduced the elastic modulus, reduced the thermal stress, and increased the toughness of the epoxy material. This new type of low stress epoxy encapsulant has great potential application in molding large IC devices when the epoxy materials are properly formulated and applied, and the stress related issues such as reduced stress and reduced thermal coefficient of expansion have been properly considered and resolved.

3.3. Polyurethanes. Polyurethanes were originally based on diisocyanates and diols or polyols (see URETHANE POLYMERS). However, more recent work has focused on the use of intermediates which are low molecular weight polyethers with reactive functional groups such as hydroxyl or isocyanate groups able to further cross-link, chain extend, or branch with other chain extenders to become higher molecular weight polyurethanes. Diamine and diol are chain extended with the prepolymer, either polyester or polyether, to form polyurethanes with urea or urethane linkages, respectively. The morphology of polyurethane is well characterized. Hard and soft segments from diisocyanates and polyols, respectively, are the key to the excellent physical properties of this material.

Bases are more widely used than acids as catalysts for polyurethane polymerization. The catalytic activity is increased with the basicity. Amines, such as tertiary alkylamines, and organic metal salts, such as tin or lead octoates, promote the reaction of isocyanate and hydroxyl functional groups in the polyurethane system and accelerate the cross-linking. However, the hydrolytic stability of the polyurethane can be affected by the catalyst and particularly the polyester polyol-based urethanes used. Uv stabilizers are usually added to reduce the radiation sensitivity of the material, especially for those products based on polyols with polybutadiene backbones which do well in hot, humid climates. In addition, polyurethane has unique high strength, high

modulus, high hardness, and high elongation. It is one of the toughest elastomers used.

High performance polyurethane elastomers are used in conformal coating, potting, and in reactive injection molding (or reaction impingement molding) of IC devices. Furthermore, rigid polyurethane foams, most often in free-foam densities of 128–288 kg/m^3 [8–18 lbs/ft^3 (pcf)], are useful for embedding complex electronic systems. The encapsulant is injected or poured as a liquid into the cavity containing the electronics. As the polymerization reactions occur, a side-reaction with water produces small bubbles and causes the urethane to foam. Usually within two minutes, the rising foam is locked into position by the cure advancement. With proper design, the rising foam pushes air out of the cavity, giving a void-free encapsulant. These materials offer weight reduction, relatively good dielectric properties, and protection from shock. They are used in a number of military ordnance systems at up to 27,000 *g*-forces.

3.4. Polyesters. Polyester is used in embedding resins for electronic components because of its low cost compared to silicones and epoxides. Polyesters, Thermoplastics are condensation products of dicarboxylic acids and dihydroxy alcohols; the reaction provides a wide range of viscosities for polyesters.

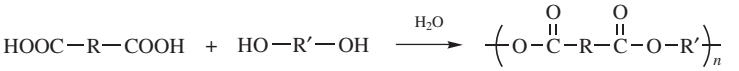

Polyesters may be saturated or unsaturated. The unsaturated polyesters contain double bonds (ethylenic groups) within the polymer backbone structure. These polyesters are cured by cross-linking the unsaturated ethylenic groups with vinyl monomers such as vinyltoluene, divinylbenzene, styrene, and dialkyl phthalate–methyl methacrylate. The reaction mechanism consists of free-radical addition across the double bond with no volatile by-products. Organic peroxides, such as dicumylperoxide and benzoperoxide, are used to promote the free-radical polymerization. Saturated polyesters are produced by the condensation of saturated dicarboxylic acids with polyhydric alcohol. Water is a by-product of the condensation. Their higher shrinkage after cure, by-product water, and high ionic impurity of the materials make polyesters inferior to silicones and epoxies and they cannot be used in critical microelectronic applications. There are electronic-grade polyesters with relatively low viscosities that are suitable for embedding of coils, as in transformers. Furthermore, free-radical-cured polyesters are popularly used for display castings.

3.5. Polysulfides. Polysulfides are organic polymers that contain sulfur in disulfide linkages (S–S), mercaptans (S–H), or thiol groups (S–R) (see POLYMERS CONTAINING SULFUR, POLY(PHENYLENE SULFIDE)). Low molecular weight polysulfides (3000–4000) may oxidatively react with free-radical reactants such as lead, tin, cobalt octoate, *p*-quinone, dicumene hydroperoxide, lead and manganese dioxides to yield rubbery flexible polysulfides with good water, gas, and moisture sealer properties. Most polysulfides have excellent adhesion to coated substrates and resistance to oxidation, solvents, and ozone. However, the electrical properties of this material are marginal as an insulator, and the dielectric constant of

the material is relatively high ($\epsilon_1 \leq 7$). It is a low cost embedding material for transformers and connector sealing, but not too common for microelectronic embedding.

3.6. Advanced Thermoplastics Materials. Thermoplastics and linear plastics of finite molecular weight that can be fabricated into very complex structures by hot melt or injection molding are different from the thermoset materials that require cross-linking to build up infinite molecular weight to form network (cross-link) structures. Advances in thermoplastic engineering materials include amorphous thermoplastics, crystalline thermoplastics, liquid crystal thermoplastics, and fluorinated thermoplastics (see POLYMERS CONTAINING SULFUR, POLY(PHENYLENE SULFIDE)).

Amorphous Thermoplastics. Polysulfone, polyethersulfone, and polyarylsulfone are examples of amorphous thermoplastics. These materials have high T_gs and can stand temperatures up to 200 °C for a long period of time.

Imide-based polymers are another class of amorphous thermoplastics.

These materials also have high thermal and oxidative stability. Flexible segments such as amide siloxane can be incorporated into the imide-based structure for hot melt or injection applications.

Crystalline Thermoplastics. These materials are actually semicrystalline, consisting of both crystalline and amorphous regions. The crystalline regions of the material provide a melting point, T_m, in the material, and the amorphous region results in a glass-transition temperature, T_g. In general, T_g is lower than T_m. Unlike amorphous plastics, crystalline plastics experience less property change at T_g. This enhances physical properties between T_g and T_m. The only drawback of this type of plastic material is the high processing temperature required for processing, usually $>T_m$. Two types of crystalline materials are usually used: ketone-based or poly(phenylene sulfide) (PPS). These materials are high performance engineering plastics, with high thermal stability, excellent chemical resistance, and superior mechanical strength.

Liquid Crystal Thermoplastics. Liquid crystal thermoplastics (LCT) have rigid, rod-like backbone structures that tightly pack to form fibrous-like crystalline chains under shear in the melting process. This highly rigid, rod-like structure requires a very high melting temperature to process (>400 °C) and creates problems in embedding electronic applications. However, copolymerization with disordered molecules results in lower melting-point materials.

These LCT materials have very high tensile and flexural strength, and excellent mechanical and chemical resistance properties.

Fluorinated Thermoplastics. Teflon, by Du Pont, a poly(tetrafluoroethylene) (TFE), is the best-known fluorinated thermoplastic. The material is highly crystalline with a melting point of 327 °C. This high melting point and its high cost limit its use in electronic embedding. However, the material has an exceptionally low dielectric constant and a dissipation factor which is ideal for microwave, high frequency, and superfast clock-rate-device-type applications. Poly(vinylidene difluoride) is another fluorinated thermoplastic that finds use in electronic embedding. Its unique piezo- and pyroelectric behavior makes it an ideal material for sensor transducer applications such as pressure, vibration, infrared, stress–strain, and impact sensing.

4. Embedding Materials Properties

The ability of a given material to perform as an electronic embedding encapsulant depends largely on its properties. Ultrapure chemical properties with a low level of mobile ions such as sodium, potassium, and chloride are essential. Furthermore, the material's electrical, mechanical, and rheological properties are critical.

4.1. Electrical Properties. Electrical properties are important for the corrosion protection of chip-on-board (COB) encapsulated devices. Accelerated temperature, humidity, and bias (THB) are usually used to test the embedding materials. Conventional accelerating testing is done at 85 °C, 85% relative humidity, and d-c bias voltage. Triple-track test devices with tantalum nitride (Ta_2N), titanium–palladium–gold (Ti–Pd–Au) metallizations with 76 μm (3 mil) line and spacing are usually used in hybrid integrated circuit (IC) encapsulant testing; however, for IC testing, 5 μm line and spacing metallization test vehicles are generally used. The triple-track test structure is usually biased at the two outer tracks, and the inner track is grounded during the 85 °C, 85% rh testing conditions. The leakage current between the outer and inner tracks is monitored periodically with testing time. Good encapsulant, with leakage current $<10^{-9}$ A after 1000 h testing, tends to have a lower leakage current with testing time. The explanation of this phenomena might be attributed to the sweeping out of the contaminant ions during testing (Fig. 4). Furthermore, the change of the resistance of the biased track with respect to the initial resistance of the biased track is also monitored during testing. The increase of

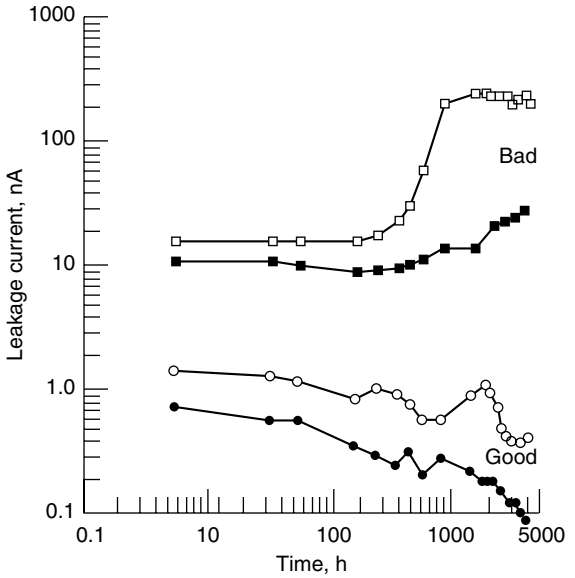

Fig. 4. Temperature–humidity–bias leakage testing of encapsulants at 85 °C, 85% rh, and 180 V bias.

the resistances is a direct measurement of the electrooxidation of the biased metallized track. Good encapsulant, with $\Delta R/R < 1\%$ after 1000 h testing, tends to have lower resistance change with time. In general, high temperature operating bias (HTOB) is also used to weed out the early failure of the imperfect encapsulated devices. Encapsulant plays a critical role in this type of successful electrical testing.

4.2. Mechanical Properties. Most of electronic IC devices are very fragile. They need strong mechanical protection from the encapsulant to retain their long-term reliability. Encapsulant must provide mechanical protection but still maintain good temperature-cycle and thermal-shock testing, which are part of the routine reliability testing of the embedding electronics.

Temperature-Cycle Testing. Normal high performance electronics require some sort of temperature-cycle testing prior to shipment. The cycling condition varies depending on the degree of reliability. In general, it varies from -30 to 130 °C. However, for military applications, 1000 cycles at -65 to 150 °C, are required. Temperature-cycle testing is done to weed out those imperfect interconnections made during IC fabrication. Embedding material must be tough and perform well in temperature-cycle testing. Low stress materials are the materials of choice.

Stress of Materials. Low stress materials are essential for dedicated device packaging. To achieve this property a low modulus material with a thermal coefficient of expansion (TCE) match is required. The stress is mainly a result of the following equation:

$$\text{stress} = k \int_{T_1}^{T_2} (\Delta TCE) E dT$$

where k is a constant, ΔTCE is the difference in thermal coefficient of expansion, E is the modulus of elasticity, and dT is the difference in temperature exclusion.

To achieve low stress embedding material, low modulus material such as silicones (elastomers or gels) and polyurethanes are usually used. Soft-domain elastomeric particles are usually incorporated into the hard (high modulus) materials such as epoxies and polyimides to reduce the stress of embedding materials. With the addition of the perfect particle size, distribution, and loading of soft domain particles, low stress epoxy molding compounds have been developed as excellent embedding materials for electronic applications.

4.3. Rheological Properties. Materials must have suitable flow properties in order to be used in production. Both Newtonian and non-Newtonian fluids and their viscoelasticity properties play a critical role in the performance of the embedding materials.

Newtonian and Non-Newtonian Materials. A Newtonian material's viscosity is shear-independent, whereas non-Newtonian materials are shear-dependent (Fig. 5). For most potting materials, a Newtonian material is preferred because the material is required to flow under all electronic components, but not be susceptible to shear. However, when flowable material is used for conformal coating applications, a non-Newtonian material with thixotropy agent added is desired since the material should flow on the electronic substrate but stop at the edge without creeping or runover at the circuitry.

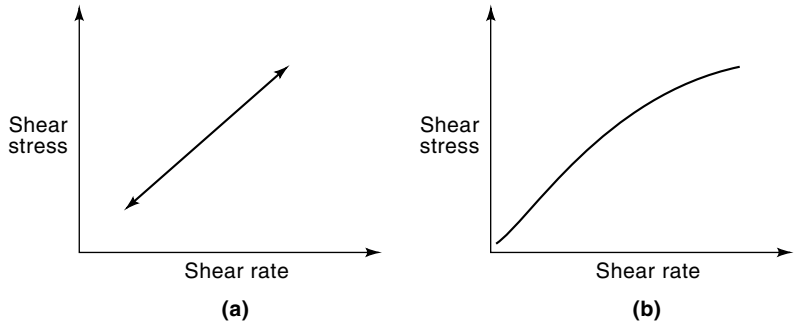

Fig. 5. Viscoelastic behavior of encapsulant materials: (**a**) Newtonian fluid; (**b**) non-Newtonian fluid.

5. Material Processes

Material processes consist of cavity-filling and saturation coating. The cavity-filling process involves molding, potting, and coating.

5.1. Molding. Molding is the most cost-effective and high performance plastic packaging method for IC devices. A polymeric resin (one of the thermosetting molding compounds) is injected into a mold and then cured, ie, the process involves two steps: (*1*) the molding compound is preheated until it melts and the resin flows through runners, gates, and finally fills up the cavities; and (*2*) the resin is cured and released from the mold in predetermined shapes. The exact control of the mold pressure, viscosity of the molten molding compound, and the delicate balance of runners, gates, and cavity designs are critical in optimizing the molded plastic IC. Finite element analysis of the plastic molding process is becoming an integral part of improving this process. Since the shear stress of the IC chip molded component could cause wire-bond sweep, device passivation cracks, top-layer metallization deformation, and multilayer oxide and nitride cracks, improved molding compounds and processes could eliminate the damage to the molded IC devices. These molding techniques are well-documented in the literature.

Pressure injection and conformal moldings are some of the current molding processes (Fig. 6). With new advances of low stress molding compounds, techniques such as transfer molding, aperture plate molding, and reactive injection molding are in production use and provide economic ways to encapsulate and package IC devices. A thorough review article and a recently published text offer excellent discussions of molding materials and processes (31,32).

5.2. Potting. Potting is the simplest cavity-filling process. It involves placing the electronic component within a container, filling the container with a liquid resin, and then curing the material as an integral part of the component. Polymeric resins, such as epoxies, silicones, and polyurethanes, are usually used as potting materials. Containers such as metal cans or rugged polymeric casings made from high performance engineering thermoplastic polymers, enhance the effectiveness of the encapsulant. Adhesion between the potted material and

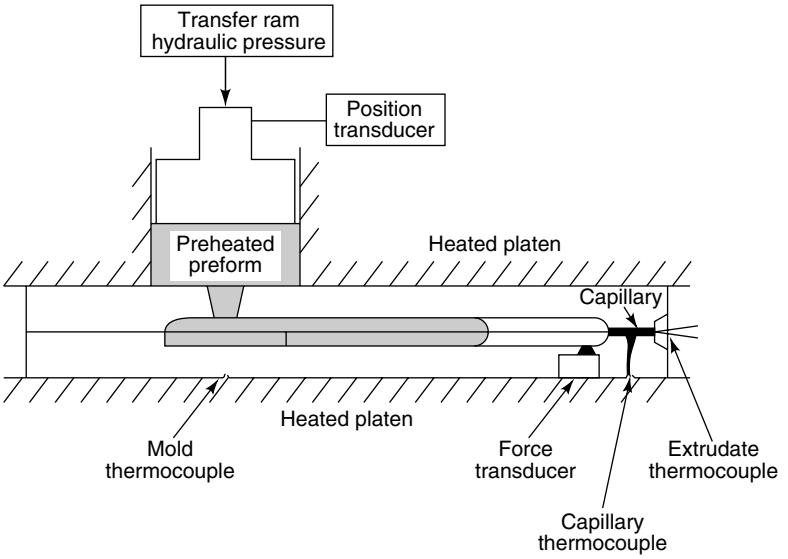

Fig. 6. Typical conformal molding process.

the casing is essential in achieving long-lasting reliable packages. In the fast-growing automated manufacturing process, rugged, machine-insertable components, such as surface-mounted chip carriers, dual-in-line (DIP), single-in-line (SIP) packages, molded and potted packages, and discrete components are highly desirable.

5.3. Casting. Casting is similar to potting, except the outer case is removed after the polymer cavity-filling process is completed and cured. No heat or pressure is applied in the process. This labor intensive casting process is not commonly used, as compared to potting and molding of modern electronic packages.

5.4. Saturation and Coating Processes. Saturation coatings consist of impregnation, dip coating, and conformal and surface coatings.

Impregnation Coating. Impregnation coating is performed by saturation of the component with a low viscosity resin; a thin film is coated on the component surface. This process is usually used with a cavity-filling or conformal coating process.

Dip Coating. Dip coating is performed by dipping the component into an encapsulating resin. The component is then withdrawn, dried, and cured. Coating thickness is usually a function of resin viscosity, withdrawal rate, and coating speed. This process also depends on the resin reactivity, curing rate, and curing temperature, etc. The dip coating process is widely used in glass-laminated printed circuit board and optical fiber coatings, where a fast-cure resin is required for the process.

Conformal and Surface Coatings. Conformal and surface coatings are the common techniques used in IC device encapsulation, and include spin coating, spray coating, and flow coating of the encapsulant onto the component. Suitable rheological properties of the encapsulant such as dynamic viscosity

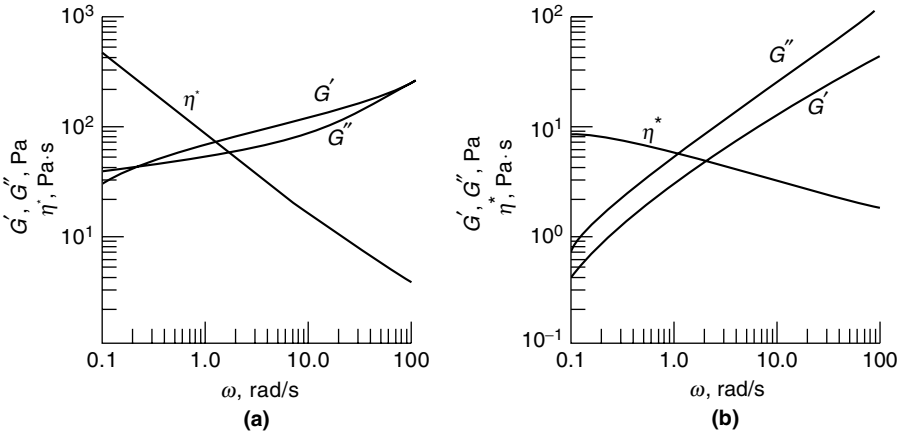

Fig. 7. Rheology of silicone encapsulants: (**a**) good material; (**b**) bad material. To convert Pa · s to P, multiply by 10. To convert Pa to dyn/cm^2, multiply by 10 (22).

(η), yield stress, G' (storage modulus), and G'' (loss modulus) are critical in obtaining a good flow-coating package (Fig. 7), especially in hybrid IC encapsulation, where the encapsulant tends to runover from the substrate and wick onto the leads of the hybrid devices. In addition, fluidized epoxy powder bed coating of single-in-line package (SIP) hybrid ICs and printed wiring boards (PWBs) are an attractive conformal coating process. Surface-mounted components on PWB are routinely encapsulated by this conformal coating process.

6. Material Curing

In order to optimize each embedding material property, complete cure of the material is essential. Various analytical methods are used to determine the complete cure of each material. Differential scanning calorimetry, Fourier transform-infrared (ftir), and microdielectrometry provide quantitative curing processing of each material. Their methods are described below.

6.1. Differential Scanning Calorimetry. A dsc measurement shows the heat flow to or from the material during its curing process. Heat capacity is measured and quantitative information regarding enthalpic transitions in a material is provided (Fig. 8). A dsc thermogram is a plot of energy supplied to or by the material as a function of temperature. The peak areas can be related to the enthalpic changes quantitatively. The T_g (glass-transition temperature) can be taken as the temperature at which one-half change in heat capacity (ΔC_p) (or the temperature at the midpoint of the change between the specific heats of the glassy and rubbery states) has occurred. Various kinetic properties can also be extracted from the dsc, eg, activation energy (E_{act}), reaction rate and reaction order. When materials are fully cured, there should be no discernable exothermic or endothermic peak as the temperature of the sample is raised at a programmed rate. In general, a sample size of a few milligrams is needed for such a dsc measurement.

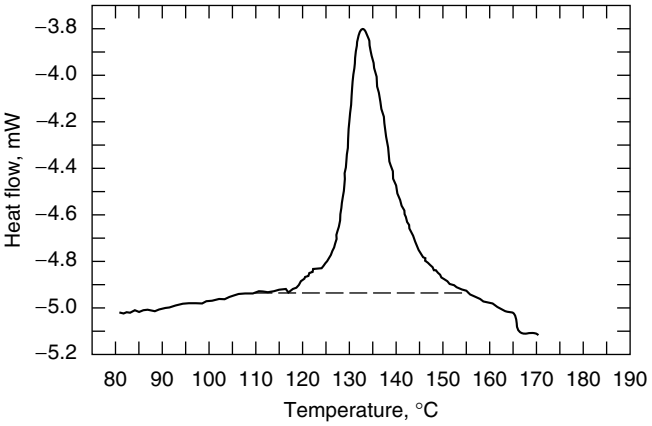

Fig. 8. Differential scanning calorimetry thermogram of a thermoset. The reaction order is 1.83, $E_{act} = 95$ kJ/mol (22.7 kcal/mol), and the heat of reaction is 6.95 J/g (1.66 cal/g).

6.2. Fourier Transform Infrared (ftir) Spectroscopy. Ftir is a sensitive tool for measuring the vibrational energy of the reactive functional groups of the encapsulant such as in heat curable silicones. For example, strong Si–H absorption at $\sim 2100\,cm^{-1}$ shows the presence of a large amount of the uncured silicone hydride. Upon hydrosilation cure, the decrease of Si–H absorption can be easily measured by its peak height or peak area integration and thus provides a useful tool for quantifying the material cure. Stabilization of the Si–H absorption is a good indication of the complete cure of the material.

6.3. Microdielectrometry. Microdielectrometry is another technique for quantitative characterization of encapsulant cure. Micromet Instruments's Eumetric System II microdielectrometer or TA Instruments's Dynamic Mechanical Thermal Analyzer with a miniature IC sensor and a wide range of frequencies

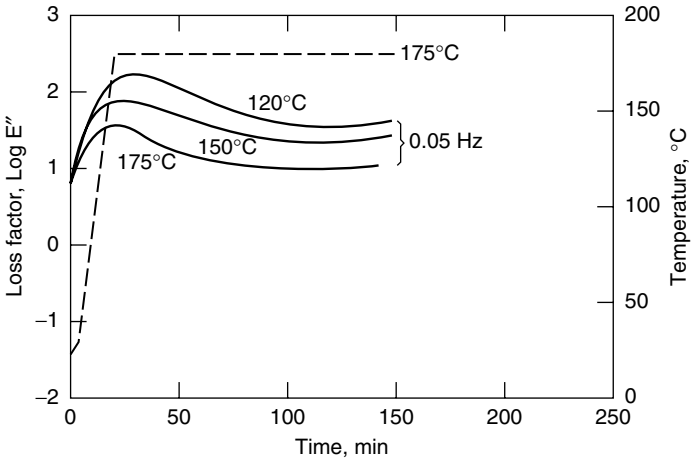

Fig. 9. Microdielectrometry study of a thermoset resin.

(from 0.05 Hz to 10 kHz) may be used to monitor the loss factor (E'') of the encapsulant. This is a sensitive technique to detect the final stage of the material cure. A thin layer of freshly prepared specimen ($\sim$500 μm thickness) is coated on the miniature IC sensor and placed inside a programmable oven. The temperature of the oven is set to the predescribed temperature, ie, 120, 150, or 175 °C, and the loss factor (E'') and dielectric constant (E') at various frequencies (0.05, 1, 100, 1,000, 10,000 Hz) are monitored periodically during the curing time (Fig. 9). When all the E' and E'' measurements are stabilized during the isothermal cure, it is a good indication of a complete cure. Low frequency (less than 0.01 Hz) sweep experiments provide a sensitive tool in quantifying the material cure (30).

7. New Technology-Aluminum-Filled Composites

7.1. Introduction. This section involves the study a novel aluminum-filled composite for embedded passive applications.

Passive components are devices that do not generate voltage or current, but their electrical characteristics are essential to form a complete circuit together with power sources and active components like ICs in an electronic system. Discrete passive components occupy more and more substrate space as the active components continue to miniaturize. It is also expected that the number of components will increase in most electronic products in next decades. Replacing discrete passive components with integral or embedded passives, in which passive components are integrated inside the substrate, has become an urgent target for next generation electronics. Embedded passives offer many advantages. Miniaturization and lower board cost are anticipated since the board area previous occupied by discrete passives are now reduced. Also, with embedded passives, internal parasitic resistance and inductance associated with surface-mounted discrete components can be suppressed due to the elimination of solder joints. Solder joints failure is one of the major reasons of electronic system failure. Embedded passives can also improve the reliability. Therefore, embedded passives not only provide increased silicon packaging efficiency and reduced assembly cost, but also improved system performance.

Among all integral passives, embedded capacitors receive special attention because of their wide range of applications. Currently surface-mounted discrete capacitors are used in all levels of electronic packing, including signal decoupling, noise suppression, filtering, tuning, bypassing, termination, and frequency determination. Embedded capacitors are particularly favored by decoupling application, because of their ability to reduce parasitic properties to an extent beyond the limit of discrete capacitors.

Embedded capacitors require development of high dielectric and low cost materials. Ceramic-filled polymer composites have been extensively investigated as candidate materials. Methodology of such approach is to combine the high dielectric constant of a ceramic filler and the low processing temperature of polymer matrices such as epoxy. The highest dielectric constant of a ceramic-polymer composite reported is 150 (at 10 kHz) (33). However, the composite requires

a very high ceramic filler loading of 85 vol%, or 98 wt%. At such high filler loading, the composite has poor adhesion to the substrate and poor other mechanical properties as well, and moreover, uniform dispersion of ceramic filler within the epoxy matrix can hardly be achieved. To solve this problem, extensive attention has been focused on a conductor–insulator composite near the percolation threshold (34–38). Percolation transition is a critical phenomenon. According to percolation theory, the properties of physical quantities such as the d-c electrical conductivity and d-c dielectric constant of a percolation system should exhibit a power-law behavior. The effective dielectric constant can be described by the following equation (37):

$$\epsilon = \frac{\epsilon_D}{|f_c - f|^q}$$

where ϵ_D is the dielectric constant of insulator, q is scaling constant, f is the percentage of the conductor, and f_c is the percolation threshold at which the conductivity of conductor-insulator composite increases dramatically when f approaches f_c from below the percolation threshold. An ultra-high dielectric constant of 500,000 in molybdenum-filled composites have been observed experimentally (37). Silver-epoxy composite materials have a high dielectric constant (>1,000) and high reliability performance suitable for embedded passive application (38). As the filler loading needed to achieve percolation is much lower for silver composites, their adhesion strength is much better compared with typical polymer–ceramic composites. However, such a system requires precise control of filler loading (0.1 vol%) and extreme uniform distribution of filler. Practically, it is impossible to fulfill such a demanding uniform distribution over a large area at all. Silver is an expensive metal and its use will increase the cost of final products.

To achieve a wider composition window suitable for industry manufacturing, Xu and wong have developed a novel low-cost aluminum-filled high dielectric constant composite. Aluminum is well known as a fast self-passivation and low-cost metal. The thin passivation layer forms a boundary layer outside of the metallic spheres, that has dramatic effects on the electrical, mechanical, and chemical behaviors of the resulting composites. Influences of aluminum particle size and filler loading on the dielectric properties of composites were studied. Due to the self-passivation nature of fine aluminum spheres, high loading level of aluminum can be used while the composite materials remain insulating. Dielectric property measurements demonstrated that, for composites containing 80 wt% 3.0 μm aluminum, a dielectric constant of 109 and a low dissipation factor of about 0.02 (at 10 kHz) were achieved. At such a loading level, materials show good processability and good adhesion to the substrate. Bulk resistivity measurement, high resolution transmission electron microscope (TEM) observations, and thermogravimetric analysis (tga) were conducted to characterize the aluminum powders. Dielectric mechanism of the materials was discussed, based on the comparison with aluminum oxide-filled composites. Bimodal aluminum-filled composites were also systematically studied, in order to increase the dielectric constant to the maximum. A revised Ouchiyaa-Tanaka equation (39) was used to calculate the maximum packing fraction. Based on the theoretical calculation, a rheology

study was performed to find the bimodal weight ratio that gives the lowest viscosity at the same loading. Such bimodal weight ratio leads to the highest loading level for the specific system. A dielectric constant of 160 (at 10 KHz) was achieved with optimized bimodal aluminum composites.

7.2. Experimental Procedures. *Material Preparation.* Epoxy resin (Epon 828) was chosen as the polymer matrix because of its ease of processing and its good compatibility with printed wiring board (PWB) manufacturing. Methylhexahydrophthalic anhydride, (MHHPA) and 1-cyanoethyl-2-ethyl-4-methylimidazole (2EMZ-CN) were used as hardener and curing catalyst, respectively. The equivalent ratio of epoxide to anhydride was set to be 1:0.85. Three untreated spherical aluminum powders were used. The average particle sizes were about 10.0 μm, 3.0 μm, and 100 nm respectively. The aluminum oxide powder, used had an average particle size of about 42 nm.

The 2E4MZ-CN was first dissolved in the MHHPA and then the Epon 828 was added into the solution. The epoxy system was carefully mixed in a centrifugal machine for two hours. To achieve uniform distribution of metal powders inside the epoxy system, a three-step mixing procedure was used. First, the composites were hand-stirred for 15 min as a premixing step, the paste from first step was then further dispersed in an ultrasonic chamber for 30 min. Finally, a high shear blender was used in order to break down the agglomeration of fine filler powders.

Capacitor Fabrication and Dielectric Measurement. A glass slide served as the bottom electrode of capacitors after being deposited with a thin layer of titanium and copper by a d-c sputterer. The composite material was coated onto the slide with bar coating method. Next, the whole sample was cured with an optimized step-curing procedure in an oven. Finally, the d-c sputterer deposited another layer of top electrode onto the material through a mask.

Dielectric measurement was conducted at the frequency of 10 kHz to 10 mHz. The dielectric constant was calculated from the measured capacitance data, according to the following equation:

$$C = \frac{\epsilon_0 \epsilon_r A}{t}$$

where ϵ_0 is the permittivity of the free space (8.854×10^{-12} F/m), A is the area of capacitor electrode, and t is the thickness of dielectric layer. ϵ_r is the dielectric constant of measured composite material.

DSC Measurement. The curing profile of epoxy system was studied by a modulated differential scanning calorimeter. Based on the curing profile of the epoxy system, three different step-curing profiles were investigated in order to determine the best curing procedure for aluminum filled composites (see Fig. 10).

The curing procedure was optimized based on three criteria. First, it should have a soft baking step to evaporate the solvent, since at high aluminum loading level, a solvent must be used in order to achieve good dispersion of aluminum particle into the matrix. According to the curing profile of epoxy system (Fig. 10), the onset temperature of curing was around 122 °C. Therefore, 120 °C was selected to be the soft baking temperature in that the curing process of epoxy is very slow at this temperature and, thus, the solvent has enough time to vaporize

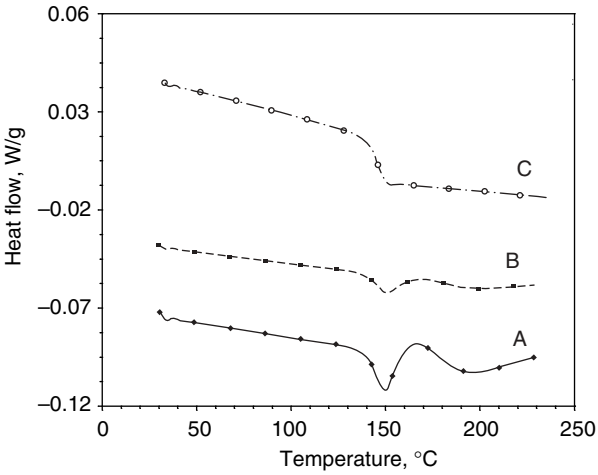

Fig. 10. Heat flow as a function of temperature of 60 wt% aluminum filled composites cured under three different step-curing profiles: A, 120 °C for 15 min, then 140 °C for 1 h; B, 120 °C for 15 min, then 145 °C for 1 h; C, 120 °C for 15 min, then 150 °C for 1 h.

without voiding. Second, the final curing temperature should be high enough to guarantee complete curing of epoxy, otherwise, the uncured portion will cause the properties of the ultimate composite to change gradually in the long run of service. Third, the curing temperature should not be too high, since high curing temperature not only leads to evaporation of the hardener, whose boiling point is less than 150 °C, but also causes the precipitation of filler particle as the viscosity decrease with the increase of curing temperature. High curing temperature also induces thermo-mechanical stress to the PWB substrate. The peak curing temperature of the epoxy system is 147 °C. Based on this, three final curing temperatures, 140 °C, 145 °C, and 150 °C were investigated. Figure 10 shows the heat flow as a function of temperature of 60 wt% aluminum-filled composites cured under three different step-curing profiles.

Nonreversible heat flow as a function of temperature is given in Figure 11. At curing temperatures of 140 °C and 145 °C, the aluminum filled composites were not completely cured. Their curing degrees were 98.4% at 140 °C, and 99.5% at 145 °C, respectively. However, curing of aluminum composites was complete at a curing temperature 150 °C, which was then chosen as the curing temperature of aluminum composites.

7.3. Results. *Unimodal Aluminum Filled Composites.* Aluminum is a fast self-passivation metal. Upon compaction, the thin passivation oxide layer forms a boundary layer outside of the metallic spheres that has dramatic effects on the electrical, mechanical, and chemical behaviors of the resulting composites. As shown in Figure 12, bulk resistivities of all three aluminum powders are in the magnitude of 10^7 ohm · cm, which corresponds to semiconducting materials and is totally different from electrically conductive aluminum metal.

After instant surface passivation at ambient conditions, aluminum particles become very stable. The weight increase of aluminum from 25 °C to 400 °C is only

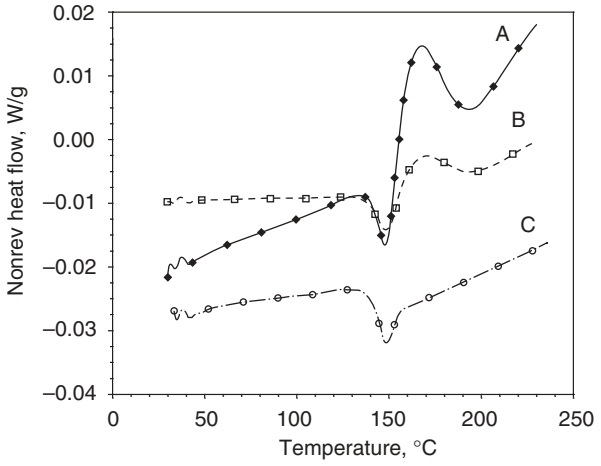

Fig. 11. Nonreversible heat flow as a function of temperature of 60 wt% aluminum filled composites cured under three different step-curing profiles: (A) 120 °C for 15 min, then 140 °C for 1 h; (B) 120 °C for 15 min, then 145 °C for 1 h; (C) 120 °C for 15 min, then 150 °C for 1 h.

about 0.07% for 3.0 μm and 10.0 μm aluminum powders, and about 0.30% for nanoaluminum powder.

Figure 13 and Figure 14 show the dielectric constant and dissipation factor of aluminum filled composites, respectively. 3.0 μm and 10.0 μm aluminum can be easily loaded up to 85 wt% in epoxy. However, for 100-nm nanoaluminum filler, it is difficult to disperse aluminum particles uniformly when filler loading is higher than 50 wt%, as is for 42 nm nanoaluminum oxide. The dielectric constant of aluminum-filled composites increases with the filler loading level, except at very high filler loading level, ie, 10.0 μm aluminum composites show a lower dielectric constant at 85 wt% than at 80 wt%. This probably is due to voiding from solvent evaporation since a large amount of solvent is required to disperse filler at such a high filler loading. For a composite filled with monodisperse

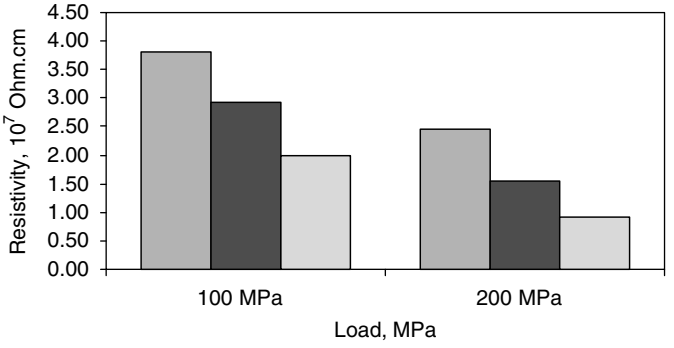

Fig. 12. Bulk resistivity of aluminum powder; ■ 10.0 micron aluminum ■ 3.0 micron aluminum ■ 100 nm aluminum.

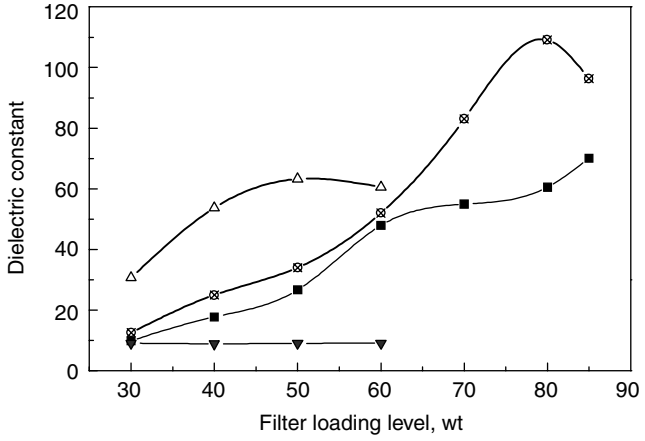

Fig. 13. Dielectric constant of aluminum filled composites as a function of filler loading (at 10 kHz); –■– 10.0 μM aluminum filled, –⊗– 3.0 μm aluminum filled, –△– 100 nm aluminum filled, –▼– 42 nm aluminum oxide filled.

spheres, the theoretical maximum volume loading is 74% (39), corresponding to 86.7 wt% for aluminum-epoxy composites. In practice, however, the packing is not this efficient. When filler loading near the theoretical volume fraction, there might be some voids present in the composite, which leads to the reduction in dielectric constant. The 3.0 μm aluminum composites have higher dielectric constant than that of the 10.0 μm aluminum composites, and the maximum dielectric constant achieved is 109 for the former and 70 for the latter. At the same filler loading, 100 nm nanoaluminum composites have higher dielectric constant than the other two kinds of aluminum composites. The highest dielectric constant is 60 at 50 wt% for nanoaluminum composites. As compared with alu-

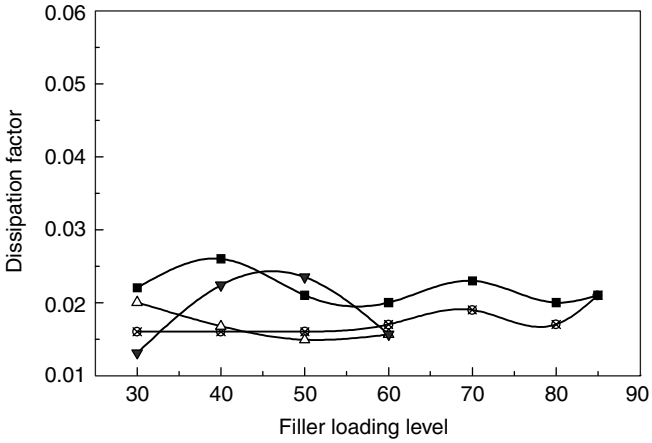

Fig. 14. Dissipation factor of aluminum-filled composites as a function of filler loading (at 10 KHz); –■– 10.0 μm aluminum filled, –⊗– 3.0 μm aluminum filled, –△– 100 nm aluminum filled, –▼– 42 nm aluminum oxide filled.

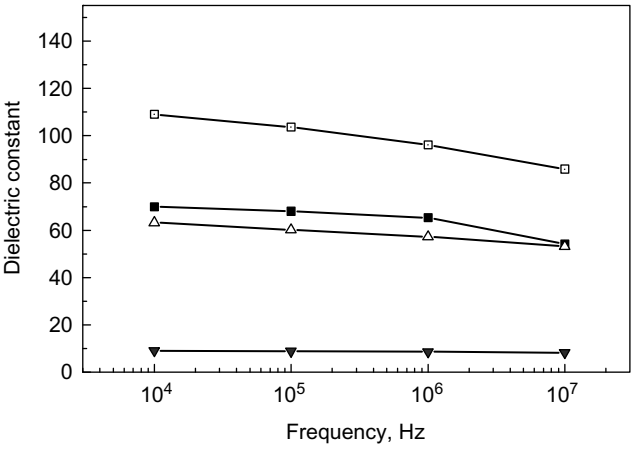

Fig. 15. Frequency dependence of aluminum-filled composites as a function of loaded filler type. The materials tested are 80 wt% 3.0 μm Al-filled composite, 80 wt% 10.0 μm Al-filled composite, 50 wt% nano Al-filled composite, and 50 wt% nano Al_2O_3-filled composite; –■– 10.0 μm aluminum, –□– 3.0 μm aluminum, –△– 100 nm aluminum, –▼– 42 nm aluminum oxide.

minum oxide-filled composites, the dielectric constant of aluminum-filled composites is much higher, which indicates they have different dielectric mechanisms. All composites studied including aluminum composites and aluminum oxide composites, show a very low dissipation factor (ca 0.02) which is desirable for embedded passive applications.

Frequency dependence of aluminum filled composites is shown in Figure 15. At a frequency below 1 MHz, the dielectric constant of aluminum filled composites is stable in terms of frequency, however, for 3.0 μm and 10.0 μm aluminum composites, a decrease in dielectric constant is observed when the test frequency increases from 1 MHz to 10 MHz. Both of nanoaluminum-filled composites and nanoaluminum oxide-filled composites show less frequency dependence at this range.

Dielectric properties of materials are based on their polarizabilities. Polarization occurs when the centers of the negative and positive charge do not coincide spatially. There are four major types of polarization that occur at specific frequencies: electronic polarization (10^{15} Hz), ionic polarization (10^{12} Hz to 10^{13} Hz), molecular or dipolar polarization (10^{11} Hz to 10^{12} Hz), and interfacial polarization (around 10^3 Hz). The first three polarization mechanisms occur at frequency above 10^{11} Hz. Interfacial polarization happens at relative lower frequency range close to the authors measurement frequencies. Interfacial polarization is due to the movement of mobile charge carriers like electrons under an applied electric field. The charge carriers become piled up at a physical barrier such as grain or phase boundaries, defects, or free surfaces. Each of the various mechanisms of polarization is dependent on the applied frequency of the electric field to the dielectric material. For the aluminum-filled composites, the major mechanism underlying is the interfacial polarization due to spatial charges. Such polarization takes place at relative lower frequency, ie, 10^3 Hz, therefore,

at low frequency (<1 MHz), aluminum composites show high dielectric constant, but when frequency increases (>1 MHz), the mobile charge cannot completely follow the oscillation of the applied electrical field, which results in the decrease of the dielectric constant and the materials show frequency dependence. The dielectric behavior of aluminum composites in the giga Hz range is being investigated.

The spatial charge carriers in aluminum composites are electrons tunneling out from the core metal inside the aluminum oxide shell. Since aluminum oxide has no such electron source as aluminum, the nanoaluminum oxide-filled composites show much lower dielectric constant, as can be seen in Figure 13. The ability of electron to tunnel through the oxide layer, which ultimately determines the dielectric properties of the corresponding composites, is directly related the thickness of aluminum oxide layer. According to Mott-Cabrera mechanism (40), the growth of aluminum oxide film shows the behavior of *n*-type semiconductor, ie, the conduction electrons in a metal core move to the conduction level of the oxide by thermionic emission or by quantum mechanical tunneling effect. The electrons then combine with oxygen adsorbed on the oxide surface and O_2^- ions are formed. A local electric field grows as the thin oxide layer behaves as a plate capacitor in which the metal core is the positive electrode and the surface of oxide layer is negative electrode. Metal ions can jump over their potential barrier, move through the oxide layer and reach the surface under the local electrical field. The thickness of oxide film increases as metal ions react with O_2^- ions at the surface. The growth of oxide film is rapid at the early stage (in pico seconds), and the film becomes saturated as the sign of the electrical potential across the oxide changes.

The thickness of oxide layer is correlated with the particle size. For bulk aluminum, the thickness of oxide is 4–5 nm at room temperature (41). With the 400 kV high resolution TEM, an oxide thickness of 2.8 nm was observed for the 100 nm aluminum powder used in this work, Figure 16 shows the micrograph of 100 nm aluminum powder from the high resolution TEM observation. Since the oxide thickness of 2.8 nm for 100 nm aluminum particle is larger than

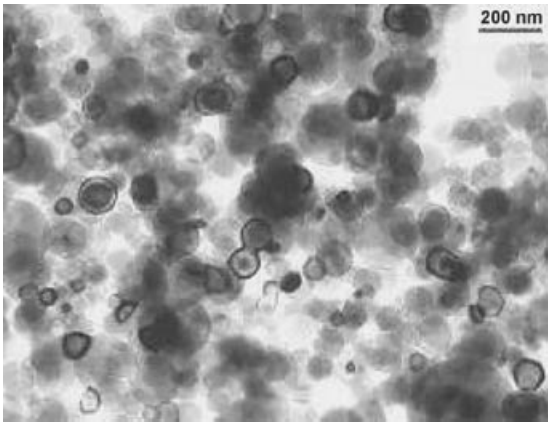

Fig. 16. High resolution TEM micrograph of 100 nm aluminum powder (400 kV).

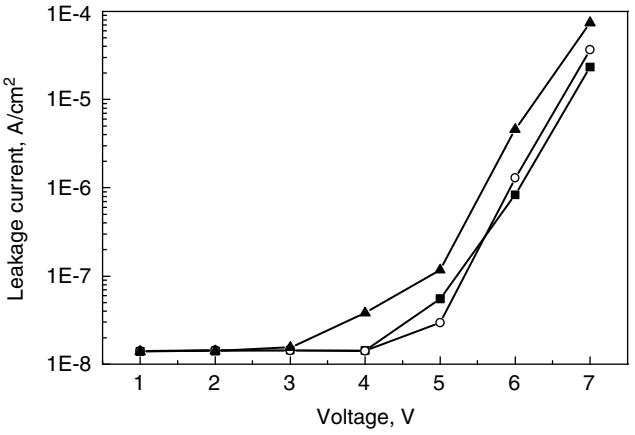

Fig. 17. Leakage current of aluminum filled composites as a function of voltage; —■— 10.0 μm aluminum filled, —○— 3.0 μm aluminum filled, —▲— 100 nm aluminum filled.

the oxide thickness of 1.0 nm for 4–12 nm aluminum particle (42) but smaller than the oxide thickness of 4–5 nm for bulk aluminum, one can draw the conclusion that the thickness of oxide film becomes smaller as the metallic particle size decreases.

From the TGA study, it is found that a larger aluminum particle size is more stable during heating in air environment. One reason for the stability is that larger particle has a relatively smaller specific surface area, which limits its contact with environment. Another reason is that the larger aluminum particle has thicker oxide layer, which can better protect the particle from further oxidation than smaller particle does. When applied with an external electrical field, thinner oxide film makes electrons in the metal core easier to tunnel through the oxide layer, thus more mobile charge carriers existing outside the thin oxide film. The smaller aluminum particle should show lower bulk resistivity than larger one, which agrees well with the experiment data in bulk resistivity measurement, as shown in Figure 12. When incorporated into a epoxy matrix, the smaller aluminum particle leads to more mobile charge carriers in the boundary between aluminum particle and epoxy matrix in the composite. Therefore, the smaller aluminum filled composites have a higher polarizability in an external electrical field, and the dielectric constant of corresponding composites is higher than the bigger particle filled composites.

Figure 17 shows the leakage current versus voltage of 80 wt% 3.0 μm aluminum-filled composite, 80 wt% 10.0 μm aluminum-filled composite, and 50 wt% 100 nm aluminum-filled composite. Leakage current increases slightly when dc bias is below 5 V, and increases quickly when voltage further increases. Under 5 V dc bias, the leakage currents are 5.5×10^{-8} A/cm^2, 3.0×10^{-8} A/cm^2, and 1.2×10^{-7} A/cm^2 respectively.

Figure 18 shows the dielectric constant of aluminum-filled composites as a function of 85 °C/85% relative humidity aging time. Samples used are 80 wt% 3.0 μm aluminum-filled composite, 80 wt% 10.0 μm aluminum-filled composite, and 50 wt% nanoaluminum-filled composite. For all samples, dielectric constant

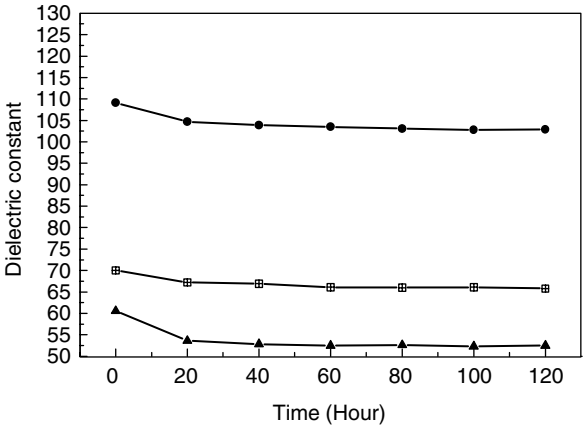

Fig. 18. Influence of 85 °C/85% relative humidity aging on the dielectric constant of aluminum-filled composites; –⊞– 10.0 μm aluminum filled, –●– 3.0 μm aluminum filled, –▲– 100 nm aluminum filled.

decreases with the aging time in the first 20 hours. After that, the dielectric constant changes very little with time. Smaller particle filler leads to bigger change in dielectric constant of composite materials than larger particle filler does. The change of dielectric constant is related with moisture absorption.

The weight gain of aluminum composites during 85 °C/85% relative humidity aging was studied. The weight gain percentage was calculated based on the resin part only in the composites. Moisture absorption is evident in the first 20 hours, as the weight gain is around 1.7 wt% during this period, however, there is almost no difference in weight gain between different-sized aluminum-filled composites.

Further oxidation of aluminum filler accounts for the difference in dielectric constant change of different-sized aluminum-filled composites. The smaller particle is more active, as found in TGA analysis, therefore, it is more readily oxidized further in 85/85 thermal humidity condition. The increased oxide layer from 85/85 treating can reduce electronic tunneling, thus, smaller number of mobile carriers present in the aged composites. Larger particle has less further-oxidation, therefore less change of dielectric constant is found.

Figure 19 shows the die shear strength of 3.0 μm aluminum-filled composites, 10.0 μm aluminum-filled composites, and nanoaluminum-filled composites. The die shear strength decreases with the increase of filler loading as the level of adhesive (epoxy resin) is reduced. Particularly, there is a dramatic decrease when the loading increases from 80 wt% to 85 wt% for 3.0 μm aluminum-filled composites and 10.0 μm aluminum-filled composites, and from 50 wt% to 60 wt% for nanoaluminum-filled composites. At 80 wt% aluminum filler loading, the die shear strength is 17.13 MPa and 17.58 MPa for 3.0 μm aluminum and 10.0 μm aluminum, respectively, which indicates the aluminum filled composites will have good adhesion to the copper layer when incorporated into the substrate structure.

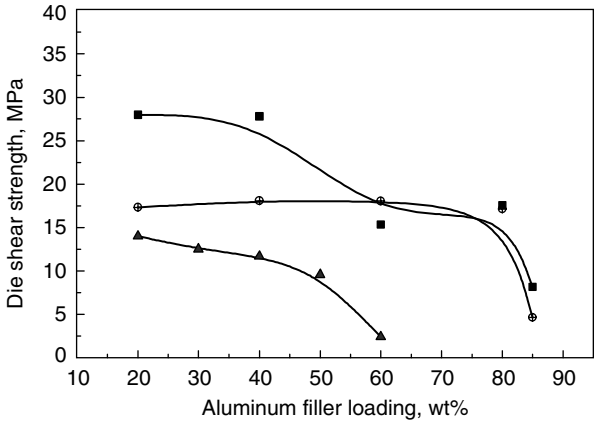

Fig. 19. Die shear strength of aluminum filled composites; —■— 10.0 μm aluminum filled, —⊗— 3.0 μm aluminum filled, —▲— 100 nm aluminum filled.

Bimodal Aluminum-Filled Composites. Bimodal aluminum-filled composites were also systematically studied, in order to increase the dielectric constant to the maximum. It is well known that polydispersity of filler size can reduce the viscosity of filled system, in particular, at high filler loading level the viscosity can be dramatically reduced by the increased particle size modality. Poslinski (43) found that a minimum viscosity could be achieved when the bimodal filler loading ratio is near the theoretical maximum packing fraction, which indicates high filler loading can be used in such system.

According to Ouchiyama and Tanaka's (44–46) model, Gupta and Seshadriz (39) developed an equation to calculate the maximum packing fraction (MPF) of polydisperse systems of spheres by taking into consideration of particle size, size distribution and modality. The equation is given as follows:

$$\phi_m = \frac{\Sigma D_i^3 f_i}{\Sigma(D_i - \bar{D})^3 + \frac{1}{\bar{n}}\Sigma\left\{(D_i - \bar{D})^3 - (D_i \sim \bar{D})^3\right\} f_i}$$

where

$$\bar{n} = 1 + \frac{4}{13}(8\phi_m^0 - 1)\bar{D}\ \frac{\Sigma(D_i + \bar{D})^2\left\{1 - \frac{3}{8}\left(\frac{\bar{D}}{D_i + \bar{D}}\right)\right\} f_i}{\Sigma\left\{D_i^3 - (D_i - \bar{D})^3\right\} f_i}$$

and

$$\bar{D} = \Sigma D_i f_i$$

Here D_i is the diameter of the i-th component, f_i is the number fraction of i-th component, and $(\phi_m{}^0$ is the maximum packing of spheres of uniform size. And the abbreviation $(D_i - \bar{D})$ is defined as:

$$(D_i - \bar{D}) = 0 \quad \text{for} \quad D_i \leq \bar{D};$$

Table 1. **Maximum Packing Fraction of Aluminum Composites**

Filler combination	MPF	Large particle	Small particle
10 μm + 3.0 μm	0.735	0.75–0.82	0.25–0.18
10 μm + 100 nm	0.891	0.76	0.24
3.0 μm + 100 nm	0.876	0.77	0.23

and

$$(D_i - \bar{D}) = D_i - \bar{D} \quad \text{for} \quad D_i \geq \bar{D}$$

In addition, the number fraction f_i can be calculated from

$$f_i = \frac{v_i/D_i^3}{\Sigma v_i/D_i^3}$$

where ν_i is the volume fraction of i-th component.

Theoretical maximum packing fraction can be obtained from calculations of the above equations. Table 1 lists the maximum packing fraction and the corresponding weight ratio of bimodal fillers for each specific system.

According to Table 1, the maximum packing fraction occurs when the volume fraction of large particle to small particle is in the range of 4:1 to 3:1. A set of weight ratios, ie, 70/30, 75/25, 76/24, 77/23, 78/22, 79/21, 80/20, and 85/15 were then chosen to perform rheology studies, in order to find the bimodal weight ratio that gives the minimum viscosity at the same loading level. All composite materials were prepared at same filler loading of 60 wt%. The experiments were performed under steady state flow procedure with parallel plate geometry.

Shear viscosity as a function of shear rate of the bimodal aluminum filled systems: 10 μm plus 3.0 μm aluminum, 10 μm plus 100 nm aluminum, and 3.0 μm plus 100 nm aluminum were studied. All materials show shear thinning behavior. At low shear rate, the viscosity of different systems are quite different, however, at high shear rate, the viscosity becomes leveled.

Figure 20 shows the viscosity of bimodal aluminum composites at shear rate $1s^{-1}$ as a function of bimodal filler weigh ratio. At same the shear rate, for all three systems, the weight ratio of 70/30 or 85/15 has higher shear viscosity than other combinations. Minimum shear viscosity is found at weight ratio 76/24 for system with 10.0 μm and 3.0 μm aluminum, at weight ratio 80/20 for system with 10.0 μm and 3.0 μm aluminum, and at weight ratio 79/21 for system with 3.0 μm and 100 nm aluminum. The weight ratio showing the lowest viscosity at the same filler loading level indicates that the highest filler loading can be obtained at such ratio for the system. These combinations of weight ratio were then selected for further dielectric studies.

Figure 21 and Figure 22 show the dielectric constant and dissipation factor of bimodal aluminum-filled composites at 10 KHz, respectively. With the optimized filler weight ratio, the highest dielectric constant obtained is 88 for 10 μm plus 3.0 μm aluminum-filled system, 136 for 10 μm plus 100 nm aluminum-filled system, and 160 for 3.0 μm plus 100 nm aluminum-filled system.

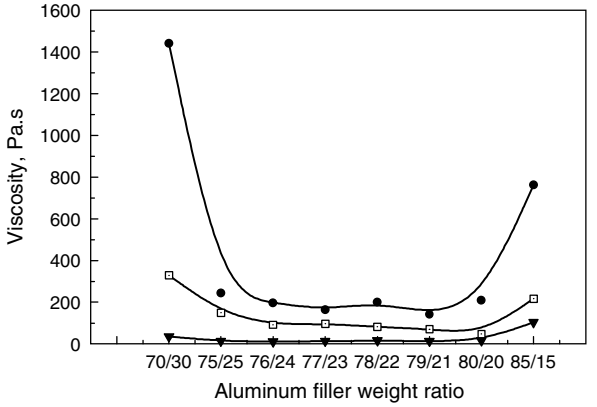

Fig. 20. Viscosity of bimodal aluminum composites at shear rate 1 s^{-1} as a function of filler weigh ratio; —▼— 10 μm + 3.0 μm, —□— 10 μm + 100 nm, —■— 3.0 μm + 100 nm.

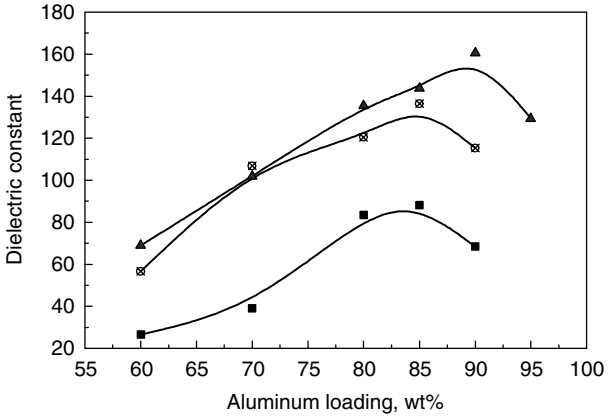

Fig. 21. Dielectric constant of bimodal aluminum filled composites (at 10 kHz); —■— 10 μm + 3.0 μm, —⊠— 10 μm + 100 nm, —▲— 3.0 μm + 100 nm.

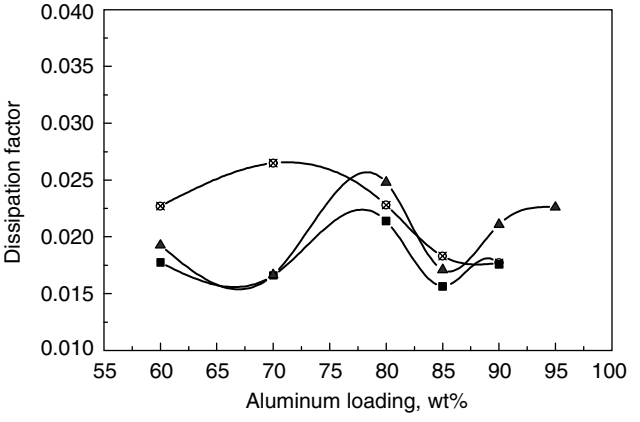

Fig. 22. Dissipation factor of bimodal aluminum filled composites (at 10 kHz); —■— 10 μm + 3.0 μm, —⊞— 10 μm + 100 nm, —▲— 3.0 μm + 100 nm.

Dissipation factors of all composites are around or below 0.02, which is desirable for embedded passive application.

7.4. Conclusions. A novel high dielectric constant composite material has been developed by using the self-passivation aluminum as filler. The thickness of passivation oxide layer formed outside the aluminum sphere determines the ultimate electrical properties of the corresponding composites. With the proper insulating oxide layer, high loading level of aluminum can be used while the composite materials remains insulated. For composites containing 80 wt% 3.0 μm aluminum a dielectric constant of 109 and low dissipation factor of about 0.02 (at 10 kHz) have been achieved. Compared with aluminum oxide-filled composites, interfacial polarization is found to be the major mechanism underlying the high dielectric constant, which is supported by bulk resistivity measurement, TGA analysis, and high resolution TEM observation. Aluminum composites have good reliability as shown in 85/85 aging test, and good adhesion towards a copper-laminated substrate as shown in die shear measurement. Bimodal aluminum-filled composites have also been systematically studied. Rheology study shows that minimum shear viscosity occurs at weight ratio 76/24 for system with 10.0 μm plus 3.0 μm aluminum, at weight ratio 80/20 for system with 10.0 μm plus 100 nm aluminum, and at weight ratio 79/21 for system with 3.0 μm plus 100 nm aluminum. Such weight ratios can provide the highest filler loading for the specific systems. Using the optimized filler weight ratio from rheology study, the highest dielectric constant obtained at 10 kHz is 88 for system filled with 10 μm plus 3.0 μm aluminum, 136 for system filled with 10 μm plus 100 nm aluminum, and 160 for system filled with 3.0 μm plus 100 nm aluminum.

8. Acknowledgments

The authors gratefully acknowledge the National Science Foundation for the financial support through grant No. NSF ECS #. 0203412. The authors acknowledge the Lindau chemicals, Inc. for their donation of MHHPA.

BIBLIOGRAPHY

"Embedding" in *ECT* 2nd ed., Vol. 8, pp. 102–116, by F. J. Modic and D. A. Barsness, General Electric Co.; in *ECT* 3rd ed., Vol. 8, pp. 877–899, by C. A. Harper, Westinghouse Electric Corp.; in *ECT* 4th ed., Vol. 9, pp. 377–393, by C. P. Wong and Paul D'Ambra, AT&T Bell Labs; "Embedding" in *ECT* (online), posting date: December 4, 2000, by C. P. Wong and Paul D'Ambra, AT&T Bell Labs.

CITED PUBLICATIONS

1. C. P. Wong, in C. P. Wong ed., *Polymers for Electric and Photonic Applications*, Academic Press, San Diego, Calif., 1993, Chapt. 4, pp. 167–214.
2. C. A. Harper, ed., *Electronic Packaging and Interconnect Handbooks*, McGraw Hill Book Co., New York, 1991.

3. M. L. Minges, ed., *Electronic Materials Handbook*, ASM International, Metals Park, Ohio, 1989.
4. R. R. Tummala and E. J. Rymaszewski, eds., *Microelectronic Packaging Handbook*, Van Nostrand Reinhold Co., Inc., New York, 1989.
5. C. P. Wong, in J. H. Lai, ed., *Polymers in Electronics*, CRC Press, Boca Raton, Fla., 1989, Chapt. 3, pp. 63–92.
6. C. P. Wong, *Application of Polymers in Encapsulation of Electronic Parts, Advances of Polymer Science*, Vol. 84, Springer-Verlag, Berlin, 1988, pp. 63–83.
7. C. P. Wong in J. I. Kroschwitz ed., *Encyclopedia of Polymer Science and Engineering*, 2nd ed., Vol. 5, John Wiley & Sons, Inc., New York, 1986, p. 638.
8. D. Seraphim, R. Ladky, and C.-Y. Li, *Principles of Electronic Packaging*, McGraw Hill Book Co., Inc., New York, 1989.
9. M. C. Volk and co-workers, *Electrical Encapsulations*, Van Nostrand Reinhold, New York, 1962.
10. W. Noll, *Chemistry and Technology of Silicone*, Academic Press, Inc., New York, 1968.
11. D. J. Shanefield and W. Colling in *Proceedings of 1st International Society for Advancement of Materials and Processing Engineers (SAMPE) Electronics Conference*, Covina, Calif., 1987, p. 70.
12. C. P. Wong in R. Jacodine, K. A. Jackson, and R. C. Sundahl, eds., *Material Research Society Symposium Proceedings*, Pittsburgh, Pa., Vol. 108, 1988, pp. 175.
13. F. N. Sinnadurai, *Handbook of Microelectronics Packaging and Interconnection Technologies*, Electrochemical Publications Limited, 1985, p. 8.
14. R. Miller in *Proceedings of the National Electronic Packaging and Production Conference (NEPCON) West*, Des Plaines, Ill., 1986, pp. 867–870.
15. C. P. Wong, *Int. J. Hybrids Microelectron.* **4**(2), 315 (1981).
16. C. P. Wong and D. E. Maurer in *Semiconductor Moisture Measurement Technology*, Special Publication 400-72, National Bureau of Standards, 1982, p. 275.
17. C. P. Wong, *Improved Room-Temperature Vulconized Silicone Elastomers as Integrated Circuit Encapsulants, Polymer Materials for Electronics Applications*, American Chemical Society Symposium Series, Washington, D.C., Nos. 184, 171, 1982.
18. H. Danielsson in *International Society for Hybrids and Microelectronics Proceedings*, Reston, Va., 1988, p. 135.
19. M. L. White, *Proc. IEEE* 27, 1610 (1969); J. H. Martin and L. D. Hanley, *IEEE Trans. Comp. Hybrids Manuf. Technol.* CHMT-4, 210 (1981).
20. R. G. Mancke, Ref. 19, 492 (1981).
21. N. Sinnardurai, *Microelectron. J.* **12**, 6 (1981).
22. C. P. Wong and D. M. Rose, *IEEE Trans. Comp. Hybrids Manuf. Technol.* CHMT-6, 485–493 (1983).
23. C. P. Wong, in *Proceedings of the IEEE 5th VLSI Packaging Workshop*, Paris, France, 1986, p. 45.
24. R. Miller, *ISHM J.* **4**, 315 (1986).
25. K. Otsuka and co-workers in *Proceedings of the International Electronic Packaging Society*, Des Plaines, Ill., 1986, p. 720.
26. K. Otsuka and co-workers, *IEEE Trans. Comp. Hybrids Manuf. Technol.* CHMT-12 (1987).
27. C. P. Wong, *Material Res. Soc. Proc.* **108**, 175 (1988).
28. C. P. Wong, J. M. Segelken, and J. W. Balde, *IEEE Trans. Comp. Hybrids Manuf. Technol.* CHMT-12(4), 419 (1989).
29. C. P. Wong, *Polymers in Electronics*, American Chemical Society Symposium Series, Washington, D.C., No. 242, 1984, Chapt. 23, p. 285.

30. C. P. Wong, *Polymer Science and Engineering Proceedings*, Vol. **55**, American Chemical Society, Washington, D.C., 1986, p. 803.
31. N. Kinjo, M. Ogata, K. Nishi, and A. Kaneda, *Adv. Polym. Sci.* **88**, 1 (1989).
32. L. T. Manzione, *Plastic Packaging of Microelectronic Devices*, Van Nostrand Reinhold, New York, 1990.
33. Y. Rao, S. Ogitani, P. Kohl, and C. P. Wong, *J. Appl. Polym. Sci.* **83**, 1084–1090 (2002).
34. D. M. Grannan, J. C. Garland, and D. B. Tanner, *Phys. Rev. Letters* **46**(5), 375–378 (1981).
35. D. S. McLachlan, I. I. Oblakova, and A. B. Pakhomov, *Physica B*, 194–196, 2001–2002 (1994).
36. Y. Song, T. W. Noh, S. Lee, and J. R. Gaines, *Physical Rev. B* **33**(2), 904–908 (1986).
37. C. Pecharromün and J. S. Moya, *Adv. Mater.* **12**(4), 294–297 (2000).
38. Y. Rao, C. P. Wong, and J. Xu, "High Dielectric Polymer Composites and Methods of Preparation Thereof," U.S. Patent Pending, 2002.
39. R. K. Gupta and S. G. Seshadri, *J. Rheol.* **30**(3), 503–508 (1986).
40. N. Cabrera and N. F. Mott, *Reports Progr. in Phys.* **12**, 163 (1948–1949).
41. N. F. Mott, *Nature* **145**, 996 (1940).
42. S. Sako, K. Ohshima, and T. Fujita, *J. Phys. Soc. Japan* **59**(2), 662–666 (1990).
43. A. J. Poslinski, M. E. Ryan, and R. K. Gupta, S. G. Seshadri, and F. J. Frechette, *J. Rheol.* **32**(B), 751–771 (1988).
44. N. Ouchiyama and T. Tanaka, *Ind. Eng. Chem. Fund.* **19**, 338–340 (1980).
45. N. Ouchiyama and T. Tanaka, *Ind. Eng. Chem. Fund.* **20**, 66–71 (1981).
46. N. Ouchiyama and T. Tanaka, *Ind. Eng. Chem. Fund.* **23**, 490–493 (1984).

C. P. WONG
JIANWEN XU
Georgia Institute of Technology